Research Article
Genetic and Metabolic Diseases

JOURNAL
OF HEPATOLOGY

Activated hepatic stellate cells and portal fibroblasts contribute to cholestatic liver fibrosis in *MDR2* knockout mice

Graphical abstract

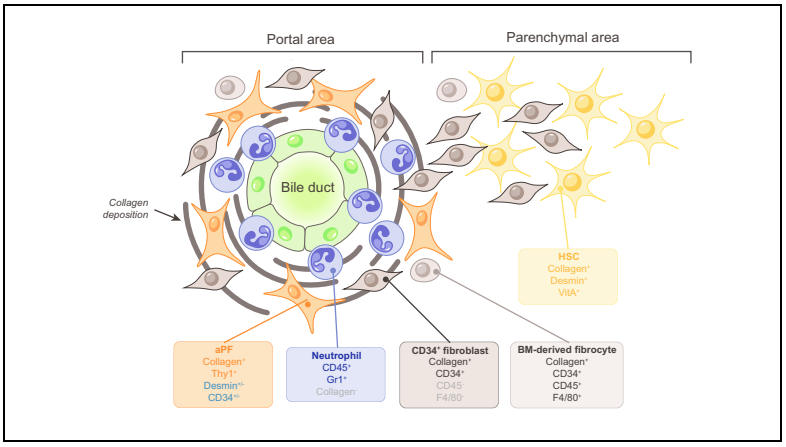

Highlights

- Hepatic myofibroblasts progressively accumulate in the livers of *Mdr2*$^{-/-}$ mice.
- Myofibroblasts mostly originate from hepatic stellate cells or portal fibroblasts.
- Meanwhile, fibrocytes minimally contribute to myofibroblasts in *Mdr2*$^{-/-}$ mice.
- In addition to collagen production, myofibroblasts serve as a source of NADPH oxidase (NOX).
- Therapeutic blocking of NOX1/4 ameliorates cholestatic fibrosis in *Mdr2*$^{-/-}$ mice.

Authors

Takahiro Nishio, Ronglin Hu, Yukinori Koyama, ..., Kojiro Taura, David A. Brenner, Tatiana Kisseleva

Correspondence

tkisseleva@ucsd.edu (T. Kisseleva)

Lay summary

Activated portal fibroblasts and hepatic stellate cells, but not fibrocytes, contributed to the production of the fibrous scar in livers of *Mdr2*$^{-/-}$ mice, and these cells can serve as targets for antifibrotic therapy in cholestatic injury. Therapeutic inhibition of the enzyme NADPH oxidase (NOX) in *Mdr2*$^{-/-}$ mice reversed cholestatic fibrosis, suggesting that targeting NOXs may be an effective strategy for the treatment of cholestatic fibrosis.

http://dx.doi.org/10.1016/j.jhep.2019.04.012
 J. Hepatol. 2019, 71, 573–585

Research Article
Genetic and Metabolic Diseases

JOURNAL OF HEPATOLOGY

Activated hepatic stellate cells and portal fibroblasts contribute to cholestatic liver fibrosis in *MDR2* knockout mice

Takahiro Nishio[1], Ronglin Hu[1], Yukinori Koyama[1,2], Shuang Liang[1], Sara B. Rosenthal[1], Gen Yamamoto[1], Daniel Karin[1], Jacopo Baglieri[1], Hsiao-Yen Ma[1], Jun Xu[1], Xiao Liu[1], Debanjan Dhar[1], Keiko Iwaisako[3], Kojiro Taura[2], David A. Brenner[1], Tatiana Kisseleva[4,*]

[1]*Department of Medicine, University of California San Diego, La Jolla, CA, USA;* [2]*Department of Surgery, Graduate School of Medicine, Kyoto University, Kyoto, Japan;* [3]*Department of Medical Life Systems, Faculty of Life and Medical Sciences, Doshisha University, Kyotanabe, Japan;* [4]*Department of Surgery, University of California San Diego, La Jolla, CA, USA*

Background & Aims: Chronic liver injury often results in the activation of hepatic myofibroblasts and the development of liver fibrosis. Hepatic myofibroblasts may originate from 3 major sources: hepatic stellate cells (HSCs), portal fibroblasts (PFs), and fibrocytes, with varying contributions depending on the etiology of liver injury. Here, we assessed the composition of hepatic myofibroblasts in multidrug resistance gene 2 knockout (*Mdr2*$^{-/-}$) mice, a genetic model that resembles primary sclerosing cholangitis in patients.

Methods: *Mdr2*$^{-/-}$ mice expressing a collagen-GFP reporter were analyzed at different ages. Hepatic non-parenchymal cells isolated from collagen-GFP *Mdr2*$^{-/-}$ mice were sorted based on collagen-GFP and vitamin A. An NADPH oxidase (NOX) 1/4 inhibitor was administrated to *Mdr2*$^{-/-}$ mice aged 12–16 weeks old to assess the therapeutic approach of targeting oxidative stress in cholestatic injury.

Results: Thy1^{+} activated PFs accounted for 26%, 51%, and 54% of collagen-GFP^{+} myofibroblasts in *Mdr2*$^{-/-}$ mice at 4, 8, and 16 weeks of age, respectively. The remaining collagen-GFP^{+} myofibroblasts were composed of activated HSCs, suggesting that PFs and HSCs are both activated in *Mdr2*$^{-/-}$ mice. Bone-marrow-derived fibrocytes minimally contributed to liver fibrosis in *Mdr2*$^{-/-}$ mice. The development of cholestatic liver fibrosis in *Mdr2*$^{-/-}$ mice was associated with early recruitment of Gr1^{+} myeloid cells and upregulation of pro-inflammatory cytokines (4 weeks). Administration of a NOX inhibitor to 12-week-old *Mdr2*$^{-/-}$ mice suppressed the activation of myofibroblasts and attenuated the development of cholestatic fibrosis.

Conclusions: Activated PFs and activated HSCs contribute to cholestatic fibrosis in *Mdr2*$^{-/-}$ mice, and serve as targets for antifibrotic therapy.

Lay summary: Activated portal fibroblasts and hepatic stellate cells, but not fibrocytes, contributed to the production of the fibrous scar in livers of *Mdr2*$^{-/-}$ mice, and these cells can serve as targets for antifibrotic therapy in cholestatic injury. Therapeutic inhibition of the enzyme NADPH oxidase (NOX) in *Mdr2*$^{-/-}$ mice reversed cholestatic fibrosis, suggesting that targeting NOXs may be an effective strategy for the treatment of cholestatic fibrosis.

Introduction

Chronic liver injury often results in liver fibrosis. The development of liver fibrosis is associated with migration and proliferation of collagen type I-producing myofibroblasts, which are not present in the normal liver. Activated myofibroblasts originate from 3 major sources: hepatic stellate cells (HSCs), portal fibroblasts (PFs), and fibrocytes.[1–4] Activated HSCs (aHSCs) were implicated in the pathogenesis of experimental toxic liver fibrosis, such as chronic CCl_4 administration and alcoholic liver disease,[1,5] while PFs are predominantly activated in response to cholestatic liver fibrosis, such as bile duct ligation (BDL).[2]

Several experimental models of cholestatic liver injury have been developed.[6] BDL causes rapid activation of PFs, especially at the onset of injury. Although the pathology resulting from BDL resembles that seen in human chronic cholestatic disease, the surgical stress and the severity of cholestatic injury limit the utility of the BDL model. The multidrug resistance gene 2 knockout (*Mdr2*$^{-/-}$, also known as *Abcb4*$^{-/-}$) mouse is another well-established model of chronic cholestatic liver injury. Deficiency of Mdr2, a canalicular phospholipid flippase, disrupts biliary phospholipid secretion, leading to the increase of potentially toxic bile acid, which induces hepatocyte damage and cholangiopathy,[7–9] which is characterized by pericholangitis and onion-skin-type periductal fibrosis, resembling the pathological features of primary sclerosing cholangitis (PSC).[10,11] Despite extensive studies,[12,13] the contribution of aHSCs and activated PFs (aPFs) to cholestatic fibrosis in *Mdr2*$^{-/-}$ mice has not been defined.

Under physiological conditions, quiescent HSCs (qHSCs) reside in the space of Disse (which is located between hepatocytes and sinusoidal endothelial cells),[1] store vitamin A, and serve as liver pericytes. QHSCs express specific markers, such as glial fibrillary acid protein (GFAP), synaptophysin, nerve growth factor p75 (NGFR1), and lecithin retinol acyltransferase (Lrat).[2,14,15] In response to toxic liver injury, HSCs downregulate the expression of vitamin A in lipid droplets, migrate to the

Keywords: Activated hepatic stellate cells; Activated portal fibroblasts; Cholestatic fibrosis.
Received 21 December 2018; received in revised form 27 March 2019; accepted 8 April 2019; available online 7 May 2019
* Corresponding author. Address: 9500 Gilman Drive, #0063, 92093 La Jolla, CA, USA.
E-mail address: tkisseleva@ucsd.edu (T. Kisseleva).

pericentral areas, and transdifferentiate into collagen type I and α-smooth muscle actin (αSMA) expressing myofibroblasts.

Portal fibroblasts, which reside around the portal area and maintain the integrity of the biliary tree and portal tract,[16] comprise a small population of fibroblasts in the liver under physiological conditions. In response to cholestatic injury, PFs proliferate, get activated, and contribute to collagen type I deposition. APFs can be distinguished from aHSCs by expression of *Thy1*, *Fibulin2*, *Elastin*, *Gremlin1*, ecto-ATPase nucleoside triphosphate diphosphohydrolase 2, mesothelin (*Msln*), and mucin 16 (*Muc16*),[2,14,16,17] and the lack of HSC markers.

Therapeutic approach to cholestatic fibrosis remains challenging; hence, liver transplantation is the only effective therapy for patients with late-stage PSC.[18] The activity of NADPH oxidase (NOX), an enzyme system that catalyzes the reduction of molecular oxygen to superoxide, plays an important role in the activation of HSCs and the development of hepatic fibrosis,[19–22] and treatment with a NOX1/4 dual inhibitor decreases both CCl_4-induced hepatotoxic fibrosis and BDL-induced cholestatic fibrosis.[23]

Here, we characterize the development of cholestatic fibrosis in *Mdr2*$^{-/-}$ mice. We determined that aPFs and aHSCs (but not fibrocytes) contribute to hepatic myofibroblasts in *Mdr2*$^{-/-}$ mice during the progression of cholestatic fibrosis. Increased expression of fibrogenic genes was associated with the upregulation of Thy1 and CD34 in aPFs. Although aPFs were in close proximity to proliferating cholangiocytes, cholangiocytes themselves did not express collagen type I. Hepatic expression of NOX was induced in *Mdr2*$^{-/-}$ mice only upon the development of liver fibrosis. Therapeutic inhibition of NOX1/4 in *Mdr2*$^{-/-}$ mice reversed cholestatic fibrosis, suggesting that targeting NOXs may be an effective strategy for the treatment of cholestatic fibrosis.

Materials and methods

Mice

BALB/c-*Mdr2*$^{-/-}$ mice (gift of Dr. Frank Lammert)[24] were crossed with collagen-α1(I)-GFP (Col^{GFP}) mice.[25] Lrat^{Cre} mice (gift of Dr. Robert Schwabe)[15] were crossed with Rosa26$^{flox\text{-}stop\text{-}flox\text{-}YFP}$ reporter mice (The Jackson Laboratory, CA, USA). The mice were housed and maintained under specific pathogen-free conditions in a standard environment with a 12-hour light–dark cycle, and fed a diet of normal chow *ad libitum*, at the animal facilities of University of California San Diego under protocol S07088, approved by the Institutional Animal Care and Use Committee.

Development of liver fibrosis and treatment with NOX1/4 inhibitor

Mdr2$^{-/-}$Col^{GFP} mice (male; BALB/c; n = 5–7/group) were sacrificed at 3, 4, 8, 12, and 16 weeks of age. Wild-type Col^{GFP} mice (male; BALB/c; n = 5) were subjected to BDL (5 days) or administration of CCl_4 (1:4 in corn oil; 200 μl; 2×/week for 3 weeks). The NOX1/4 inhibitor (GKT137831; Genkyotex S.A., France)[23] was administered *in vivo* (20 or 60 mg/kg, or vehicle, 20 doses, oral gavage) to *Mdr2*$^{-/-}$ mice (male; BALB/c; n = 6–8/group) from age 12 to 16 weeks old.

Bone-marrow transplantation

Mdr2$^{-/-}$ mice (male; BALB/c; 4 weeks old; n = 6–8/group) were lethally irradiated (12 Gy) and i.v. reconstituted with the donor Col^{GFP} bone-marrow (BM) cells (1×10^7). The recipient *Mdr2*$^{-/-}$ mice were sacrificed at 16 weeks of age.

Histology and immunohistochemistry

Formalin-fixed livers were embedded in paraffin or optimal cutting temperature compound, and stained with Sirius Red or antibodies for immunohistochemistry. The positive area was quantified using ImageJ (National Institutes of Health, MD, USA) (see Supplementary materials).

Flow cytometry

Non-parenchymal cell fraction was isolated from *Mdr2*$^{-/-}$Col^{GFP} mice (4, 8, and 16 weeks old) using the pronase/collagenase method, as described.[26] GFP$^+$vitaminA$^+$ aHSCs and GFP$^+$vitaminA$^-$ aPFs were quantified and sort purified using FACSAria™ II (BD Biosciences, CA, USA).

Quantitative real-time PCR (qPCR) and RNA sequencing analysis

Total RNA was extracted using RNeasy® columns (Qiagen, MD, USA). Expression levels of selected genes (for primers, see Supplementary Table S1) were calculated after normalization to hypoxanthine guanine phosphoribosyl transferase (*HPRT*) by using the ΔΔCt method. RNA sequencing (RNAseq) analysis was performed using the non-parenchymal cell fraction, which was sort purified from 16-week-old *Mdr2*$^{-/-}$Col^{GFP} mice (see Supplementary materials).

Western blot

Western blot analysis was performed on liver tissue lysates that were separated by SDS-PAGE and transferred to nitrocellulose membranes (see Supplementary materials).

Statistical analysis

Data are mean ± SD. Differences between groups were compared using ANOVA, followed by the Tukey-Kramer test. A p value of <0.05 was considered significant. JMP Pro 11 (SAS Institute, Cary, NC, USA) software was used for all statistical analyses.

Results

Development of fibrosis in *Mdr2*$^{-/-}$ mice is associated with inflammation, oxidative stress, and ductular reaction

Progression of cholestatic liver fibrosis was analyzed in 4-, 8-, 12-, and 16-week-old *Mdr2*$^{-/-}$ mice. Extracellular matrix (ECM) deposition was observed in livers of *Mdr2*$^{-/-}$ mice as early as 4 weeks of age, and reached maximum at 12–16 weeks, as demonstrated by Sirius Red staining (Fig. 1A and B), which was accompanied by expression of fibrogenic genes (*Col1a1*, *αSMA*, *Desmin*, *TIMP1*, and *TGFβR1* mRNA; Fig. 1C) and inflammatory genes (*F4/80*, *IL-1β*, and *IL-6* mRNA; Fig. 1D). Age-dependent ECM deposition in *Mdr2*$^{-/-}$ mice correlated with increased upregulation of aHSC markers (*Desmin*, *α-SMA*, and *TIMP1* mRNA), and aPF markers (*Thy1*, *Msln*, *Muc16*, *CD34*, and *Fibulin2* mRNA, with the exception of elastin, in which the expression peaked at 4 weeks of age; Fig. 1E). Expression of NOX genes (*NOX1*, *NOX2*, and *NOX4* mRNA; Fig. 1F) and cholangiocyte markers (*CK19* and *Sox9* mRNA; Fig. 1G) followed a similar trend, suggesting that the activation of hepatic myofibroblasts in *Mdr2*$^{-/-}$ mice positively correlates with the age-dependent development of oxidative stress, hepatic inflammation, and ductular proliferation.

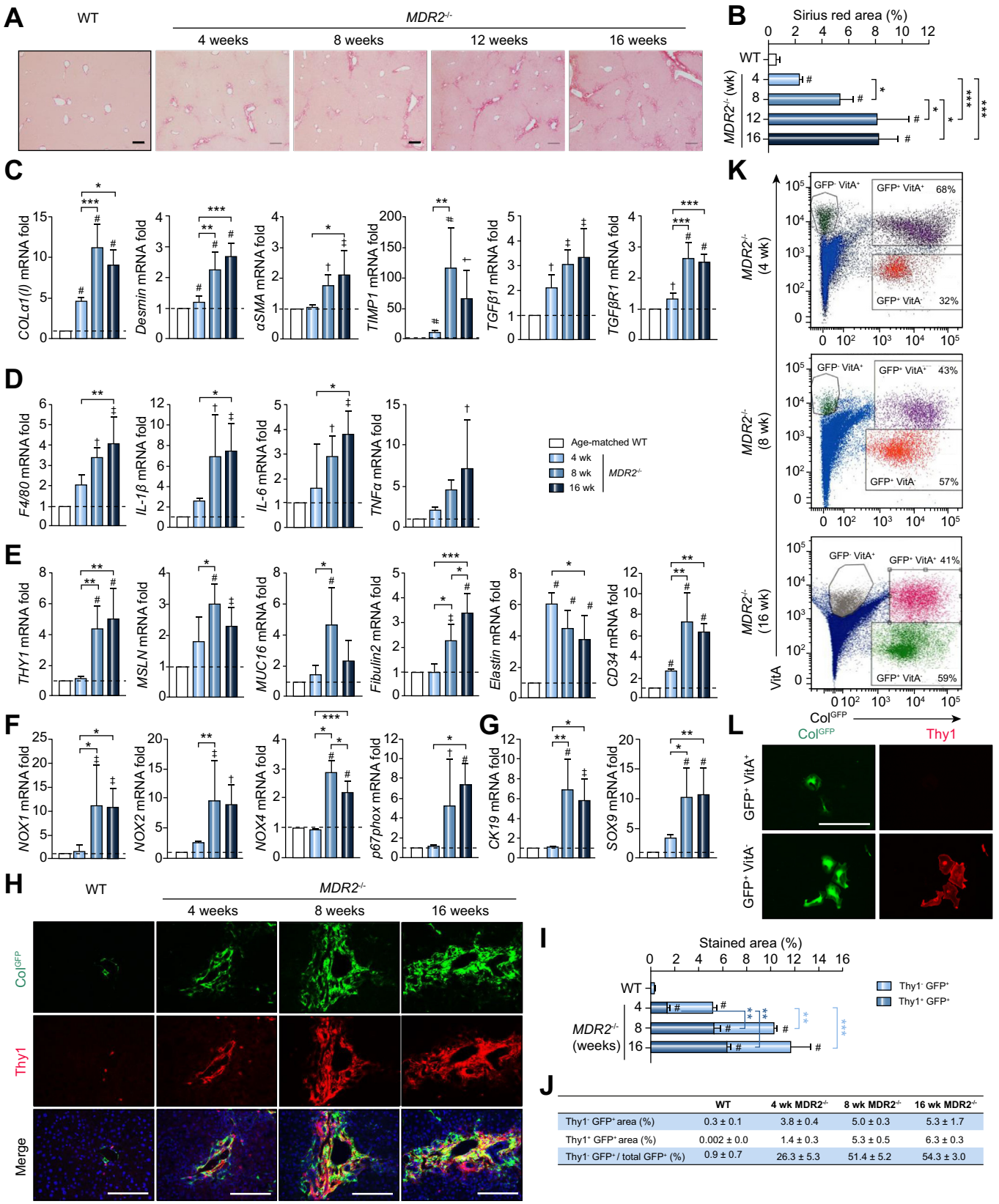

Fig. 1. APFs and HSCs contribute to the progression of cholestatic fibrosis in *Mdr2*$^{-/-}$ mice. Livers from 4-, 8-, 12-, and 16-week-old *Mdr2*$^{-/-}$ mice and age-matched WT littermates were analyzed. (A) Sirius Red staining, scale bar: 200 μm. (B) Positive area was calculated as percent. (C) Expression of fibrogenic markers, (D) inflammatory genes, (E) aPF markers, (F) *NOX* genes, and (G) cholangiocyte markers were analyzed by qPCR. Data are fold induction *versus* age-matched WT littermates. (H) Staining for Col^{GFP} and Thy1. Scale bar: 100 μm. (I and J) The composition of GFP$^+$ myofibroblasts (100%) was calculated as percent of Thy1$^+$GFP$^+$ (yellow) and Thy1$^-$GFP$^+$ (green) area. (K and L) Non-parenchymal fraction was isolated from *Mdr2*$^{-/-}$Col^{GFP} mice. GFP$^+$±Vitamin A$^+$ cells were sort purified. (K) Representative dot plots and the percent of Vit.A$^+$ and Vit.A$^-$ in GFP$^+$ cells (100%). (L) Staining for Thy1. Scale bar: 100 μm. n = 5–7 mice per age group, mean ± SD, †p <0.05, ‡p <0.01, #p <0.001 *versus* WT; *p <0.05, **p <0.01, ***p <0.001, by ANOVA. aPF, activated portal fibroblast; HSC, hepatic stellate cell; NOX, NADPH oxidase; WT, wild-type.

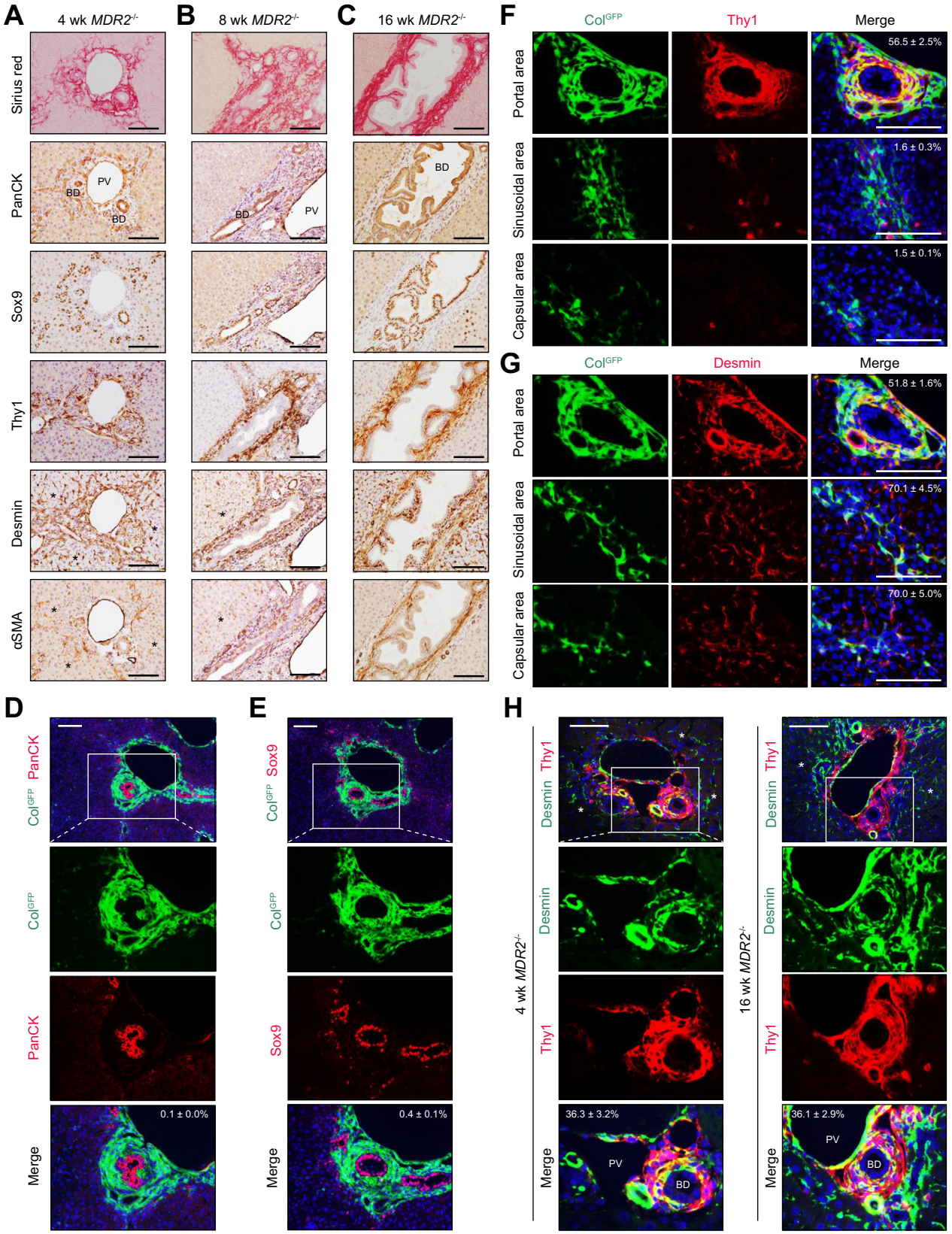

Fig. 2. Pathological features of liver injury in 4-, 8-, and 16-week-old *Mdr2*$^{-/-}$ mice. Serial liver sections from (A) 4-, (B) 8-, and (C) 16-week-old *Mdr2*$^{-/-}$ mice were stained with Sirius Red, PanCK, Sox9, Thy1, Desmin, or αSMA. Asterisks: HSCs. (D) Livers from 8-week-old *Mdr2*$^{-/-}$Col^{GFP} mice were stained for PanCK, (E) Sox9, (F) Thy1, and (G) Desmin. (H) Livers from *Mdr2*$^{-/-}$ mice were stained for Desmin and Thy1. Asterisks: HSCs. Scale bar: 100 μm. n = 5–7 per age group, mean ± SD. BD, bile duct; HSC, hepatic stellate cell; PV, portal vein.

Collagen type I-expressing myofibroblasts emerge in the livers of *Mdr2*$^{-/-}$ mice

To visualize activated myofibroblasts, *Mdr2*$^{-/-}$ mice were crossed with collagen1-α(I)-GFP reporter mice (in which all Collagen Type I expressing cells are labeled in real time with GFP)[25] to generate *Mdr2*$^{-/-}$Col^{GFP} mice. Myofibroblasts first emerged in the livers of 4-week-old *Mdr2*$^{-/-}$Col^{GFP} mice (and contributed to 5.2% of the total liver area), and were increased depending on the progression of fibrosis (up to 10.3% area of the total liver area at 8 weeks old, and 11.6% at 16 weeks old; Fig. 1H and I). Next, the composition of hepatic myofibroblasts was analyzed in *Mdr2*$^{-/-}$Col^{GFP} mice.

Thy1^{-}GFP^{+} and Thy1^{+}GFP^{+} myofibroblasts comprise the major populations of fibrogenic myofibroblasts in the livers of *Mdr2*$^{-/-}$Col^{GFP} mice

Livers from 4-, 8-, and 16-week-old *Mdr2*$^{-/-}$Col^{GFP} mice were immunostained for the aPF marker, Thy1. Compared to the total GFP^{+} myofibroblast area (considered as 100%), Thy1^{+} aPFs were progressively activated (ranging from 26% to 54% in the livers of 4- and 16-week-old *Mdr2*$^{-/-}$ mice; Fig. 1I and J). In turn, the number of Thy1^{-}GFP^{+} cells increased with age in *Mdr2*$^{-/-}$ mice, but their relative contribution to myofibroblasts declined (from 73% to 45% of the total GFP^{+} myofibroblasts in the livers of 4- and 16-week-old *Mdr2*$^{-/-}$ mice, respectively), suggesting that aHSCs and aPFs are the major contributors to ECM-producing myofibroblasts in *Mdr2*$^{-/-}$ mice.

Similar results were obtained using flow cytometry for vitamin A (Vit.A) and collagen1-α(I)-GFP myofibroblasts.[2] AHSCs were identified by simultaneous expression of Vit.A and Col^{GFP}, while GFP^{+} aPFs lacked the expression of Vit.A. Vit.A^{+}GFP^{+} aHSCs comprised 68% of GFP^{+} myofibroblasts (100%) in the livers of 4-week-old *Mdr2*$^{-/-}$ mice, but only 41% in livers of 16-week-old *Mdr2*$^{-/-}$ mice. This effect was attributed to the rapid expansion of Vit.A^{-}GFP^{+} aPFs (Fig. 1K and L), since their contribution to total GFP^{+} myofibroblasts was increased from 32% in livers of

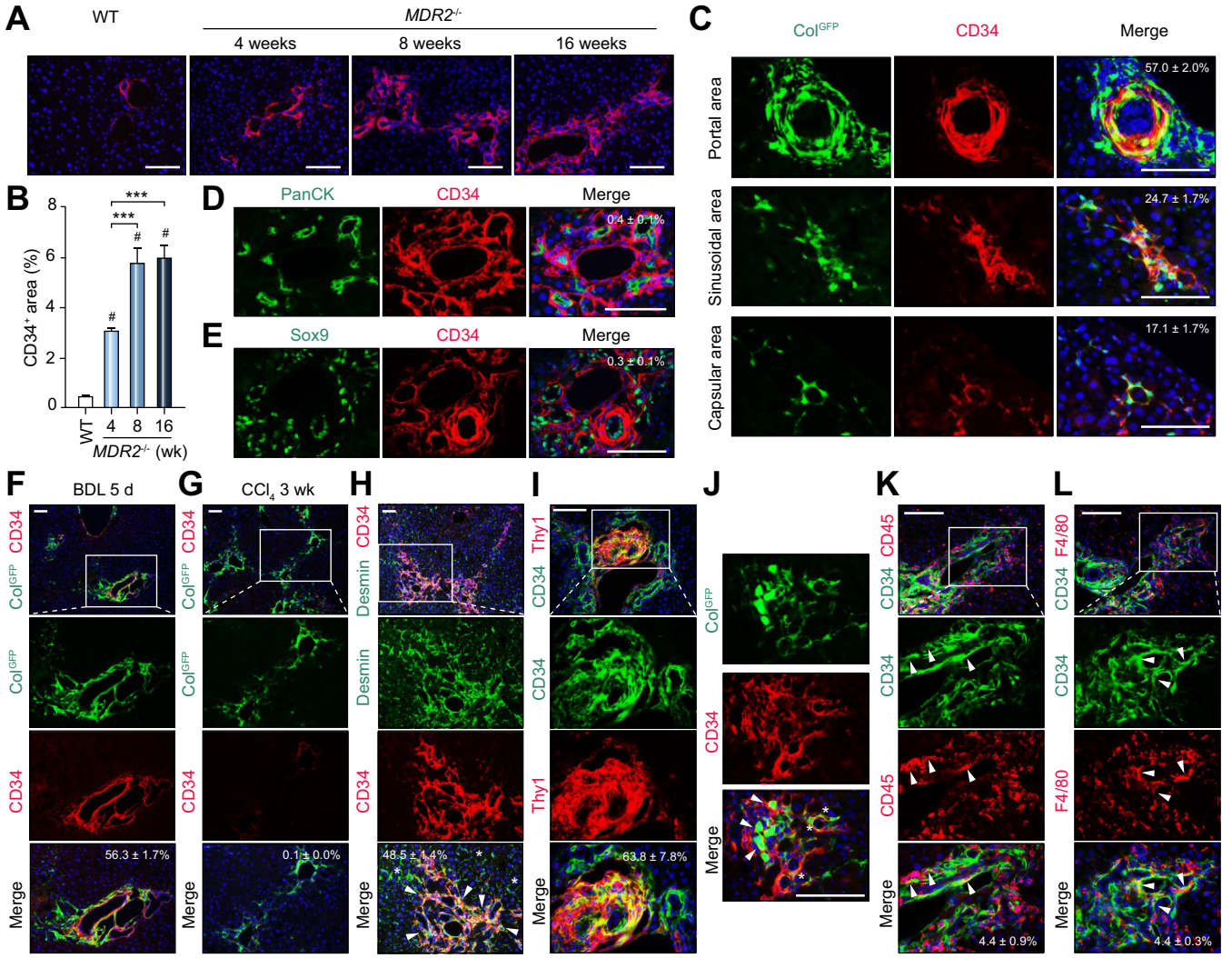

Fig. 3. Subset of Thy1^{+} aPFs co-express CD34. (A) Livers from 4-, 8-, and 16-week-old *Mdr2*$^{-/-}$ mice were stained for CD34. Scale bar: 100 μm. (B) Positive area was calculated as percent. (C) Livers from 8-week-old *Mdr2*$^{-/-}$ mice were stained for Col^{GFP} and CD34, (D) CD34 and PanCK, and (E) CD34 and Sox9. Scale bar: 100 μm. (F) Livers from BDL (5 days)-injured Col^{GFP} mice and (G) from CCl_4-injured (3 weeks) Col^{GFP} mice were stained for CD34. Scale bar: 200 μm. (H–L) Livers from 8-week-old *Mdr2*$^{-/-}$ mice were stained. Scale bar: 100 μm. (H) Staining for Desmin and CD34, and (I) CD34 and Thy1. Arrows: Desmin^{+}CD34^{+} cells. Asterisks: HSCs. (J) Staining for Col^{GFP} and CD34. Arrows: GFP^{+}CD34^{+} fibrocytes. Asterisks: GFP^{+} CD34^{+} myofibroblasts. (K) Staining for CD34 and CD45, and (L) CD34 and F4/80. n = 5–7 per age group, mean ± SD. $^{\dagger}p$ <0.05, $^{\ddagger}p$ <0.01, $^{\#}p$ <0.001 *vs.* WT; $^{*}p$ <0.05, $^{**}p$ <0.01, $^{***}p$ <0.001, by ANOVA. BDL, bile duct ligation; WT, wild-type.

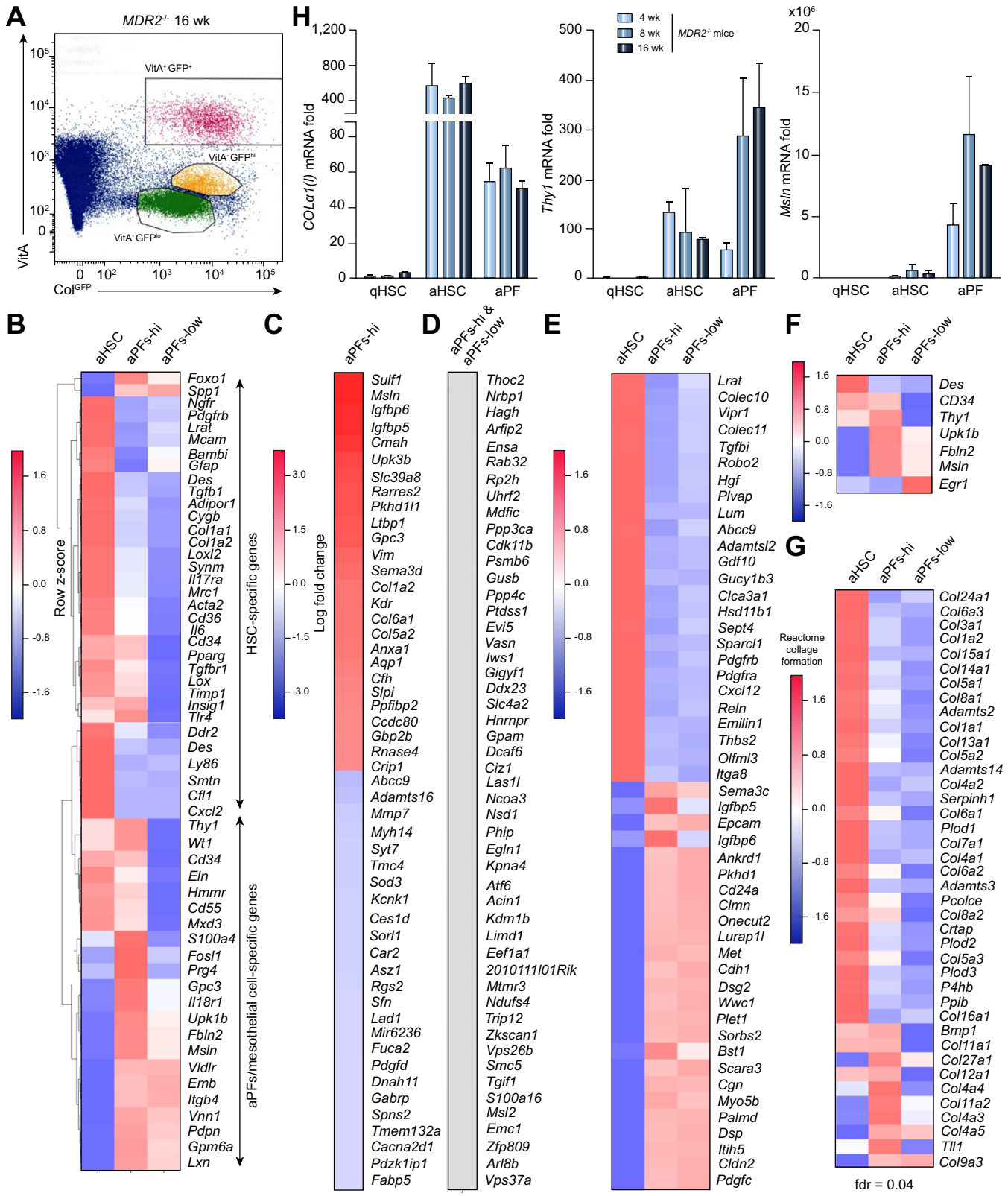
A
MDR2-/- 16 wk
VitA+ GFP+
VitA- GFPhi
VitA- GFPlo
VitA
ColGFP
H
COLa1(I) mRNA fold
Thy1 mRNA fold
Msln mRNA fold
4 wk
8 wk
16 wk
MDR2-/- mice
qHSC
aHSC
aPF
B
aHSC
aPFs-hi
aPFs-low
Row z-score
HSC-specific genes
aPFs/mesothelial cell-specific genes
Foxo1
Spp1
Ngfr
Pdgfrb
Lrat
Mcam
Bambi
Gfap
Des
Tgfb1
Adipor1
Cygb
Col1a1
Col1a2
Loxl2
Synm
Il17ra
Mrc1
Acta2
Cd36
Il6
Cd34
Pparg
Tgfbr1
Lox
Timp1
Insig1
Tlr4
Ddr2
Des
Ly86
Smtn
Cfl1
Cxcl2
Thy1
Wt1
Cd34
Eln
Hmmr
Cd55
Mxd3
S100a4
Fosl1
Prg4
Gpc3
Il18r1
Upk1b
Fbln2
Msln
Vldlr
Emb
Itgb4
Vnn1
Pdpn
Gpm6a
Lxn
C
aPFs-hi
Log fold change
Sulf1
Msln
Igfbp6
Igfbp5
Cmah
Upk3b
Slc39a8
Rarres2
Pkhd1l1
Ltbp1
Gpc3
Vim
Sema3d
Col1a2
Kdr
Col6a1
Col5a2
Anxa1
Aqp1
Cfh
Slpi
Ppfibp2
Ccdc80
Gbp2b
Rnase4
Crip1
Abcc9
Adamts16
Mmp7
Myh14
Syt7
Tmc4
Sod3
Kcnk1
Ces1d
Sorl1
Car2
Asz1
Rgs2
Sfn
Lad1
Mir6236
Fuca2
Pdgfd
Dnah11
Gabrp
Spns2
Tmem132a
Cacna2d1
Pdzk1ip1
Fabp5
D
aPFs-hi & aPFs-low
Thoc2
Nrbp1
Hagh
Arfip2
Ensa
Rab32
Rp2h
Uhrf2
Mdfic
Ppp3ca
Cdk11b
Psmb6
Gusb
Ppp4c
Ptdss1
Evi5
Vasn
Iws1
Gigyf1
Ddx23
Slc4a2
Hnrnpr
Gpam
Dcaf6
Ciz1
Las1l
Ncoa3
Nsd1
Phip
Egln1
Kpna4
Atf6
Acin1
Kdm1b
Limd1
Eef1a1
2010111I01Rik
Mtmr3
Ndufs4
Trip12
Zkscan1
Vps26b
Smc5
Tgif1
S100a16
Msl2
Emc1
Zfp809
Arl8b
Vps37a
E
Lrat
Colec10
Vipr1
Colec11
Tgfbi
Robo2
Hgf
Plvap
Lum
Abcc9
Adamtsl2
Gdf10
Gucy1b3
Clca3a1
Hsd11b1
Sept4
Sparcl1
Pdgfrb
Pdgfra
Cxcl12
Reln
Emilin1
Thbs2
Olfml3
Itga8
Sema3c
Igfbp5
Epcam
Igfbp6
Ankrd1
Pkhd1
Cd24a
Clmn
Onecut2
Lurap1l
Met
Cdh1
Dsg2
Wwc1
Plet1
Sorbs2
Bst1
Scara3
Cgn
Myo5b
Palmd
Dsp
Itih5
Cldn2
Pdgfc
F
Des
CD34
Thy1
Upk1b
Fbln2
Msln
Egr1
G
Reactome collage formation
Col24a1
Col6a3
Col3a1
Col1a2
Col15a1
Col14a1
Col5a1
Col8a1
Adamts2
Col1a1
Col13a1
Col5a2
Adamts14
Col4a2
Serpinh1
Col6a1
Plod1
Col7a1
Col4a1
Col6a2
Adamts3
Pcolce
Col8a2
Crtap
Plod2
Col5a3
Plod3
P4hb
Ppib
Col16a1
Bmp1
Col11a1
Col27a1
Col12a1
Col4a4
Col11a2
Col4a3
Col4a5
Tll1
Col9a3
fdr = 0.04

4-week-old *Mdr2*$^{-/-}$ mice to 57–59% in livers of 16-week-old *Mdr2*$^{-/-}$ mice. We concluded that both aHSCs and aPFs critically contribute to cholestatic fibrosis. Age-dependent activation of aHSCs and aPFs was further evaluated using histological analysis of *Mdr2*$^{-/-}$ mice.

Thy1^{+} aPFs serve as a significant source of ECM in *Mdr2*$^{-/-}$ mice and human cholestatic injury

The pathological features of liver injury were first examined in 4-week-old *Mdr2*$^{-/-}$ mice. The onset of cholestatic fibrosis was associated with the accumulation of Thy1^{+} and Desmin^{+} cells around the portal area, and displayed typical "onion-skin-like" fibrosis surrounding PanCK^{+} and Sox9^{+} cholangiocytes (Fig. 2A). We also observed proliferation of small Sox9^{+} bile ducts around Thy1^{+} aPFs. Immunostaining of serial sections revealed that the area of ECM deposition overlapped mostly with the Thy1^{+} area, suggesting that aPFs significantly contribute to the fibrous scar at 4 weeks of age.

At 8 weeks of age, areas positive for Thy1, Desmin, and α-SMA were markedly enlarged and correlated with increased ECM deposition in portal areas of these mice (Fig. 2B). At this age, expression of PanCK and Sox9 mostly overlapped, and was indicative of maturation of proliferating bile ducts. A similar, but more severe, pathology was observed in livers of 16-week-old *Mdr2*$^{-/-}$ mice, and was associated with the formation of a more compact fibrous scar and further activation of Thy1^{+} and Desmin^{+} myofibroblasts, whereas the immunoreactivity for αSMA was observed in the portal area, *e.g.* in fibrotic regions and in basal membranes underlying biliary epithelium (Fig. 2C).

To support our findings in *Mdr2*$^{-/-}$ mice, we validated the contribution of aPFs to myofibroblasts in human cholestatic disease using immunostaining of human liver sections (Supplementary Fig. S1). In human livers with cholestatic injury, Thy1^{+} cells accumulated in the area corresponding to ECM deposition and surrounding the CK19^{+} cholangiocytes. Notably, the Thy1^{+} area mostly overlapped with the Msln^{+} area, indicating that Thy1^{+}Msln^{+} aPFs contribute to human cholestatic fibrosis.

APFs surround the bile duct and express Desmin and Thy1

Previous reports suggested that injured cholangiocytes can produce Collagen Type I.[27] Here, we examined if PanCK^{+} and/or Sox9^{+} bile ducts upregulate Collagen Type I in 8-week-old *Mdr2*$^{-/-}$Col^{GFP} mice. Despite close proximity to Thy1^{+} aPFs, neither PanCK^{+} nor Sox9^{+} cholangiocytes expressed collagen1-α(I)-GFP (Fig. 2D and E), indicating that cholangiocytes do not contribute to ECM deposition. The majority of Thy1^{+} aPFs accumulated in the portal area, while Desmin^{+}GFP^{+} aHSCs were mostly located in the hepatic acini or capsular areas (Fig. 2F). Surprisingly, Desmin positive staining was also observed in the portal areas populated with aPFs (Fig. 2G). Furthermore, immunoreactivity for Desmin and Thy1 was co-localized in 30–40% of GFP^{+} portal myofibroblasts, while parenchymal and sinusoidal GFP^{+} HSCs were stained positive only for Desmin (Fig. 2H). Similar results were obtained in 4- and 16-week-old *Mdr2*$^{-/-}$ mice, suggesting that anti-Desmin antibodies might not discriminate between aHSCs and aPFs in livers of *Mdr2*$^{-/-}$ mice.

To address this question, cholestatic injury was induced in HSC-specific Lrat^{YFP} mice[15] (generated by crossing Lrat^{Cre} and Rosa26^{YFP} mice) via ligation of the common bile duct (BDL; 5 days). Similarly, Lrat^{YFP}-labeled cells were stained positive not only for Desmin^{+}Thy1^{-} HSCs, but also for Desmin^{-}Thy1^{+} aPFs (Supplementary Fig. S2), and exhibited a distribution pattern similar to that observed in *Mdr2*$^{-/-}$ mice. Our data imply that Lrat^{Cre} mice are suited for lineage tracing of both aHSCs and aPFs (due to Lrat expression during embryonic development). We also concluded that a subset of Mdr2-deficient aPFs upregulates Desmin. Therefore, additional markers that discriminate aPFs from aHSCs are needed.

CD34^{+} aPFs contribute to cholestatic fibrosis in *Mdr2*$^{-/-}$ mice

In an attempt to identify additional markers of aPFs that can be used for immunohistochemical studies, expression of CD34 on aPFs and aHSCs was evaluated. Transmembrane phosphoglycoprotein CD34, a member of the sialomucin family, is expressed by a variety of cells, including hematopoietic and endothelial cells, as well as mesenchymal progenitors and aPFs.[2] Here, we demonstrate that CD34^{+} was strongly expressed in Col^{GFP+} aPFs upon the development of cholestatic fibrosis in *Mdr2*$^{-/-}$ mice (Fig. 3A and B; Supplementary Fig. S3A). Upregulation of CD34 mRNA also positively correlated with an increased expression of other aPF-specific markers (*Thy1*, *Msln*, *Muc16*, *Fibulin2*; Fig. 1D). CD34^{+} cells accumulated predominantly in the portal (57%) and sinusoidal (24%) areas, and were scattered throughout the capsular (17%) area (Fig. 3C; Supplementary Fig. S4A). CD34^{+} staining did not overlay with PanCK^{+} and/or Sox9^{+} cells (Fig. 3D and E), suggesting that CD34 marks a population of aPFs in the livers of *Mdr2*$^{-/-}$ mice. In support, a population of CD34^{+} aPFs was detected in the livers of BDL-injured (but not CCl_4-injured) Col^{GFP} mice (Fig. 3F and G). Our data are in concordance with previous reports demonstrating that aPFs minimally contribute to CCl_4-induced liver fibrosis[2] (Supplementary Fig. S4B). The majority of CD34^{+} cells co-expressed Thy1 (63%) and Desmin (48%), and exhibited a fibroblast-like spindle shape in the livers of *Mdr2*$^{-/-}$ mice (Fig. 3H and I; Supplementary Fig. S3A). Hence, a small fraction of CD34^{+}GFP^{+} cells (4%) exhibited a fibrocyte-like shape (Fig. 3J), and co-expressed CD45 and F4/80 (Fig. 3K and L), suggesting that these cells might derive from BM fibrocytes.

AHSCs exhibit a more fibrogenic phenotype than aPFs

To further dissect the contribution of aHSCs and aPFs to fibrosis, Vit.A^{+}GFP^{+} aHSCs and Vit.A^{-}GFP^{+} aPFs (with high [hi] and low expression of GFP, for comparison based on the degree of

Fig. 4. Gene expression profiling of aHSCs and aPFs isolated from *Mdr2*$^{-/-}$ mice. (A) Non-parenchymal fraction was isolated from livers of 16-week-old *Mdr2*$^{-/-}$Col^{GFP} mice (n = 5 mice combined), Vit.A^{+}GFP^{+} aHSCs, Vit.A^{-}GFP^{hi}, and Vit.A^{-}GFP^{low} aPFs were sort purified and analyzed by RNAseq for (B) expression of HSC- and aPF- signature genes (rows are grouped with hierarchical clustering); (C) 25 most upregulated and 25 most downregulated genes in Vit.A^{-}GFP^{hi} aPFs compared to Vit.A^{-}GFP^{low} PFs; (D) 50 most similarly expressed genes in Vit.A^{-}GFP^{hi} and Vit.A^{-}GFP^{low} PFs; (E) most upregulated and downregulated genes in Vit.A^{+}GFP^{+} aHSCs compared to Vit.A^{-}GFP^{hi} and Vit.A^{-}GFP^{low} PFs. An average expression filter of 4 log(counts/million) was applied before calculating the log fold change to filter out likely false positives. (F) Heatmaps displaying signature gene expression in Vit.A^{+}GFP^{+} aHSCs compared to Vit.A^{-}GFP^{hi} and Vit.A^{-}GFP^{low} PFs. (G) Using gene set enrichment analysis on the msigdb set of canonical pathways, gene expression in Reactome collagen formation pathway was significantly upregulated in HSCs compared to PF samples. Heatmap colors indicate the relative expression levels in each gene; false discover rate <0.3; fdr = 0.04. (H) qPCR analysis of selected gene expression in isolated aHSCs and aPFs isolated from 4-, 8-, and 16-week-old *Mdr2*$^{-/-}$ mice (see Fig. 1K). Data are fold induction *versus* qHSCs from 4-week-old *Mdr2*$^{-/-}$Col^{GFP} mice. aHSC, activated hepatic stellate cell; aPF, activated portal fibroblast; qHSC, quiescent hepatic stellate cell; RNAseq, RNA sequencing.

activation) were sort purified (Fig. 4A) from livers of 16-week-old *Mdr2*$^{-/-}$ mice, and their gene expression profile was analyzed by RNAseq. As expected, Vit.A^{+}GFP^{+} aHSCs expressed typical HSC markers (*Lrat*, *Pdgfrb*, *Desmin*, and *GFAP*) and lacked expression of aPFs (*Msln*, *Glipican3*, *Fibulin2*, and *Uroplakin1B*; Fig. 4B). In turn, Vit.A^{-}GFP^{hi} aPFs expressed markers of aPFs (but lacked *Desmin*, *Lrat*, and *GFAP*). Slight upregulation of Thy1, Wt1, and CD34 mRNA was observed in aHSCs compared to qHSCs, while these markers were downregulated in Vit.A^{-}GFP^{low} aPFs compared to Vit.A^{-}GFP^{hi} aPFs. In addition, expression of *Msln*, *Glipican3*, *Fibulin2*, *Uroplakin*, *Vimentin*, *Col6a1*, *Col5a2* mRNA, and other genes was also reduced in Vit.A^{-}GFP^{low} aPFs (Fig. 4C), suggesting that Vit.A^{-}GFP^{low} aPFs exhibit a less activated phenotype compared to Vit.A^{-}GFP^{hi} aPFs, consistent with their higher collagen GFP expression. Despite these differences, the majority of genes were similarly expressed in Vit.A^{-}GFP^{hi} and Vit.A^{-}GFP^{low} aPFs (Fig. 4D and E), which suggests that these 2 populations originate from the same cell type at different stages of activation. In support, the expression of CD34 has been linked to maturation of tissue fibroblasts.[28]

Furthermore, high expression of early growth response 1; intermediate expression of *Upk1bm*, *Fbln2*, and *Msln*; and low expression of *CD34* and *Thy1* mRNA distinguished Vit.A^{-}GFP^{low} aPFs from Vit.A^{-}GFP^{hi} aPFs and Vit.A^{+}GFP^{+} aHSCs (Fig. 4F). When Reactome pathways were compared, aHSCs and both populations of aPFs expressed genes associated with ECM deposition (see Supplementary Tables S2–4), which is consistent with their myofibroblast phenotypes. High expression of *Col1a1*, *Col1a2*, and other fibrogenic genes was observed mostly in aHSCs. Unlike BDL-activated aPFs,[2] Vit.A^{-}GFP^{hi} aPFs in Mdr2-deficient mice expressed less *Col1a1* than aHSCs (Fig. 4H), but almost exclusively upregulated *Bmp1*, *Col27a1*, *Col11a2*, *Col4a3*, and *Tll1* mRNA (Fig. 4G). Based on the gene expression profile, we concluded that aHSCs serve as a major source of ECM in the livers of 16-week-old *Mdr2*$^{-/-}$ mice.

Minor contribution of BM-derived fibrocytes in *Mdr2*$^{-/-}$ mice

CD34^{+} fibrocytes were implicated in the pathogenesis of cholestatic fibrosis in *Mdr2*$^{-/-}$ mice.[29] In accord, a small number of Col^{GFP+} cells co-expressing CD34^{+}, CD45, and F4/80 (2–4%), designated as fibrocytes, were scattered throughout portal, sinusoidal, and capsular areas in the livers of *Mdr2*$^{-/-}$ mice (Fig. 5A–C; Supplementary Fig. S3B). To directly assess the contribution of BM-derived fibrocytes to collagen type I-producing cells/myofibroblasts in livers of *Mdr2*$^{-/-}$ mice, BM from donor Col^{GFP} mice was transplanted into lethally irradiated recipient 4-week-old *Mdr2*$^{-/-}$ mice. Recipient *Mdr2*$^{-/-}$ mice were sacrificed at 16 weeks of age, and livers were analyzed for the presence of GFP^{+}, CD45^{+}, and F4/80^{+} cells (Fig. 5D). Although BM-derived Col^{GFP+} fibrocytes migrated to the livers of recipient *Mdr2*$^{-/-}$ mice, they retained a fibrocyte-like round shape, and contributed to neither Desmin^{+} nor CD34^{+} myofibroblasts (Fig. 5E and F; Supplementary Fig. S5), suggesting that Col^{GFP+} fibrocytes minimally contribute to fibrogenic myofibroblasts

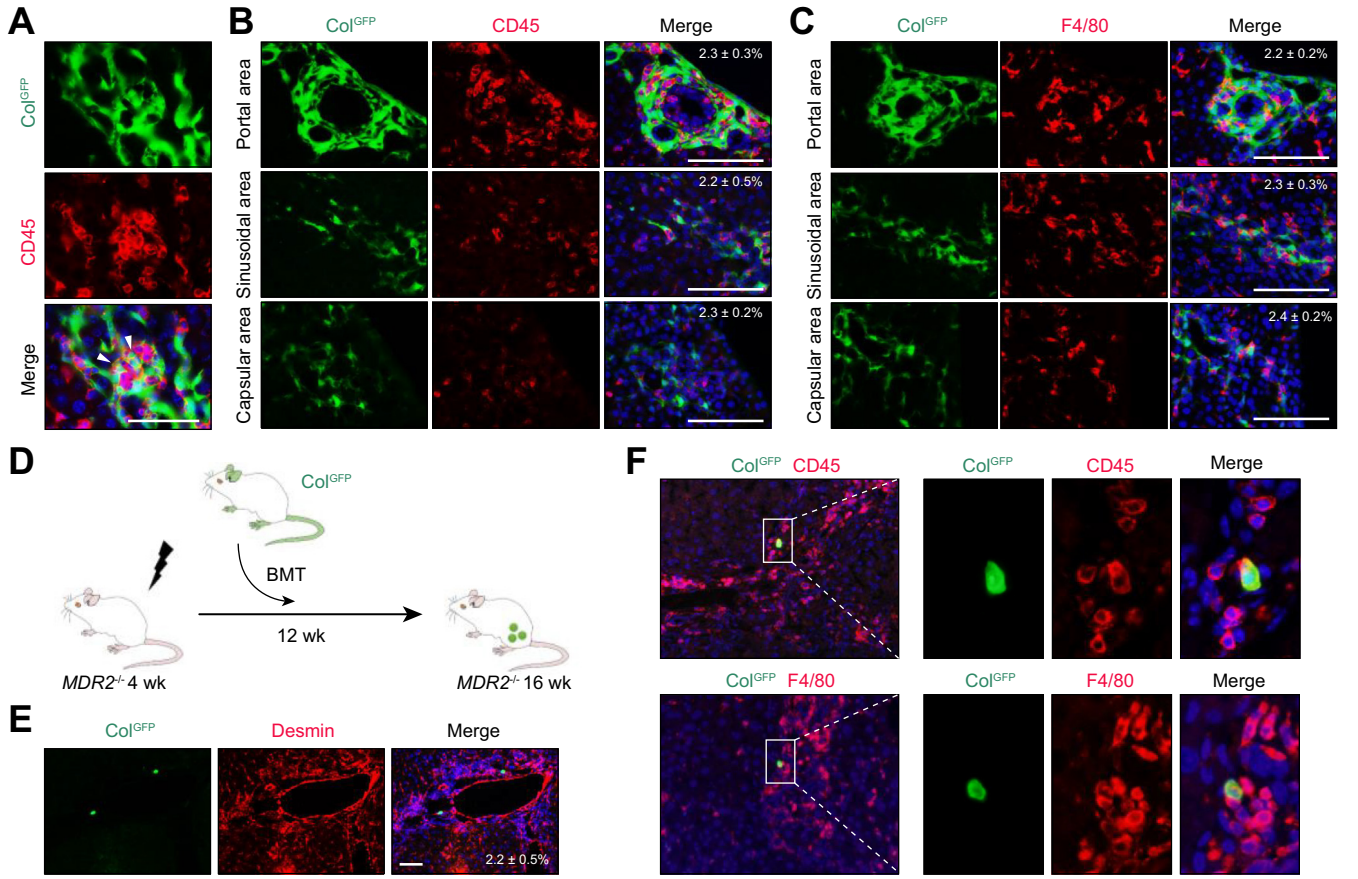

Fig. 5. BM-derived fibrocytes minimally contribute to myofibroblasts in *Mdr2*$^{-/-}$ mice. (A) Livers from 16-week-old *Mdr2*$^{-/-}$Col^{GFP} mice were stained for CD45. Arrows: GFP^{+} CD45^{+} fibrocytes. (B) Livers from 8-week-old *Mdr2*$^{-/-}$Col^{GFP} mice were stained for CD45 or (C) F4/80. (D) Bone-marrow transplantation: lethally irradiated 4-week-old *Mdr2*$^{-/-}$ mice were transplanted with Col^{GFP} BM and sacrificed at 16 weeks of age. (E) Livers were stained for Col^{GFP} and Desmin, and (F) Col^{GFP} and CD45, or F4/80. Scale bar: 100 μm; n = 6–8 per group; mean ± SD. BM, bone marrow.

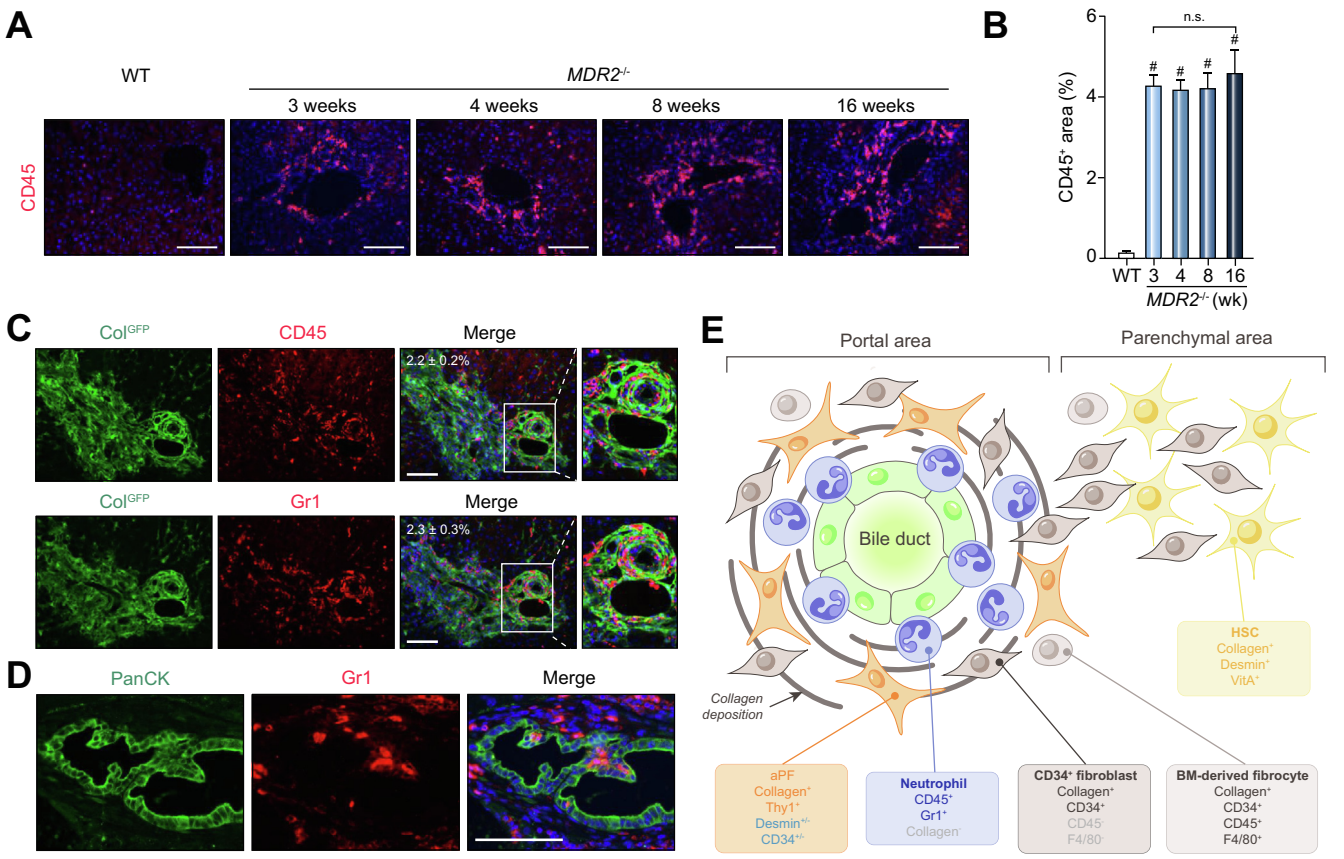

Fig. 6. CD45$^+$ Gr1$^+$ neutrophils populate portal area in livers of *Mdr2*$^{-/-}$ mice. (A) Livers from 3-, 4-, 8-, and 16-week-old *Mdr2*$^{-/-}$ mice were stained for CD45. (B) Positive area was calculated as percent. (C) Livers from 8-week-old *Mdr2*$^{-/-}$ mice were stained for Col^{GFP} and CD45, or Gr1 (serial sections), and (D) PanCK and Gr1. Scale bar: 100 μm; n = 5–7 per age group; mean ± SD. †*p* <0.05, ‡*p* <0.01, #*p* <0.001 *vs.* WT. (E) Schematic summary: cells contributing to cholestatic fibrosis in *Mdr2*$^{-/-}$ mice. aPF, activated portal fibroblast; BM, bone marrow; HSC, hepatic stellate cell; NS, not significant by ANOVA; WT, wild-type.

in livers of *Mdr2*$^{-/-}$ mice. Meanwhile, the composition of CD45$^+$ cells in the livers of *Mdr2*$^{-/-}$ mice was further analyzed.

CD45$^+$Gr1$^+$ neutrophils migrate into a portal area in the early stage of *Mdr2*$^{-/-}$ cholestatic injury

Immunostaining with anti-CD45 antibody detected a flux of BM-derived cells into the livers of *Mdr2*$^{-/-}$ mice as early as 3 weeks of age, which persisted throughout the 16 weeks of age (Fig. 6A and B). Based on the timeline, we concluded that recruitment of CD45$^+$Gr1$^+$ cells (at 3 weeks of age; Supplementary Fig. S6A) precedes the activation of PFs (4 weeks of age) and the development of fibrogenic responses in *Mdr2*$^{-/-}$ mice. Remarkably, at 4 weeks of age, the expression pattern of CD45$^+$ and Gr1$^+$ cells overlapped. CD45$^+$ and Gr1$^+$ cells were located between Col^{GFP+} myofibroblasts, and were incorporated into the fibrous scar (Fig. 6C). CD45$^+$ or Gr1$^+$ cells did not express Col^{GFP} (except a 2–4% population of BM-derived fibrocytes; Fig. 5) or CD3 in livers of 4-week-old *Mdr2*$^{-/-}$ mice (Supplementary Fig. S6B), suggesting that the majority of CD45$^+$ cells were neutrophils/granulocytes. Notably, some CD45$^+$ and Gr1$^+$ cells also infiltrated the structures of the bile ducts, and some Gr1$^+$ cells were scattered between cholangiocytes (Fig. 6D and E).

Progression of cholestatic fibrosis is associated with upregulation of NOX1 and NOX4 in livers of *Mdr2*$^{-/-}$ mice

Therapeutic approaches to treat cholestatic fibrosis remain limited. The activity of NOX, an enzyme system that catalyzes the reduction of molecular oxygen to superoxide, plays an important role in the activation of HSCs and macrophages, and promotes the development of hepatic fibrosis.[19,22] In support, strong induction of *NOX* genes was associated with the activation of myeloid cells and myofibroblasts, especially in 12- to 16-week-old *Mdr2*$^{-/-}$ mice (Fig. 1F). The RNAseq analysis also confirmed the expression of *NOX4*, *Cyba* (p22phox), *Cybb* (NOX2), and *Noxo1* in aPFs, and *Cyba*, *Ncf2* (p67phox), *Cybb*, and *Ncf1* (p47phox) in aHSCs (Supplementary Fig. S7). When livers of 16-week-old *Mdr2*$^{-/-}$ mice were examined, the expression of *4-HNE* (a marker of lipid peroxidation, which reflects oxidative stress) was highly upregulated in hepatocytes (in centrilobular area; Supplementary Fig. S8A), cholangiocytes, Thy1$^+$ cells, CD34$^+$ cells, and CD45$^+$ cells (in the portal area; Supplementary Fig. S8B). We hypothesized that blocking of the NOX pathway might attenuate or reverse cholestatic fibrosis in 12- to 16-week-old *Mdr2*$^{-/-}$ mice.

Administration of NOX1/4 inhibitor attenuates cholestatic fibrosis in *Mdr2*$^{-/-}$ mice

In an attempt to identify a novel therapeutic strategy to suppress cholestatic injury of hepatocytes and cholangiocytes, and prevent the activation of BM-derived neutrophils and fibrogenic myofibroblasts in *Mdr2*$^{-/-}$ mice, 12-week-old *Mdr2*$^{-/-}$ mice were treated with a NOX1/4 inhibitor for 4 weeks (GKT137831: 20 or 60 mg/kg, oral gavage, 5×/week, total 20 doses; Fig. 7A). Livers of *Mdr2*$^{-/-}$ mice were analyzed at 16 weeks of age. The administration of NOX1/4 inhibitor

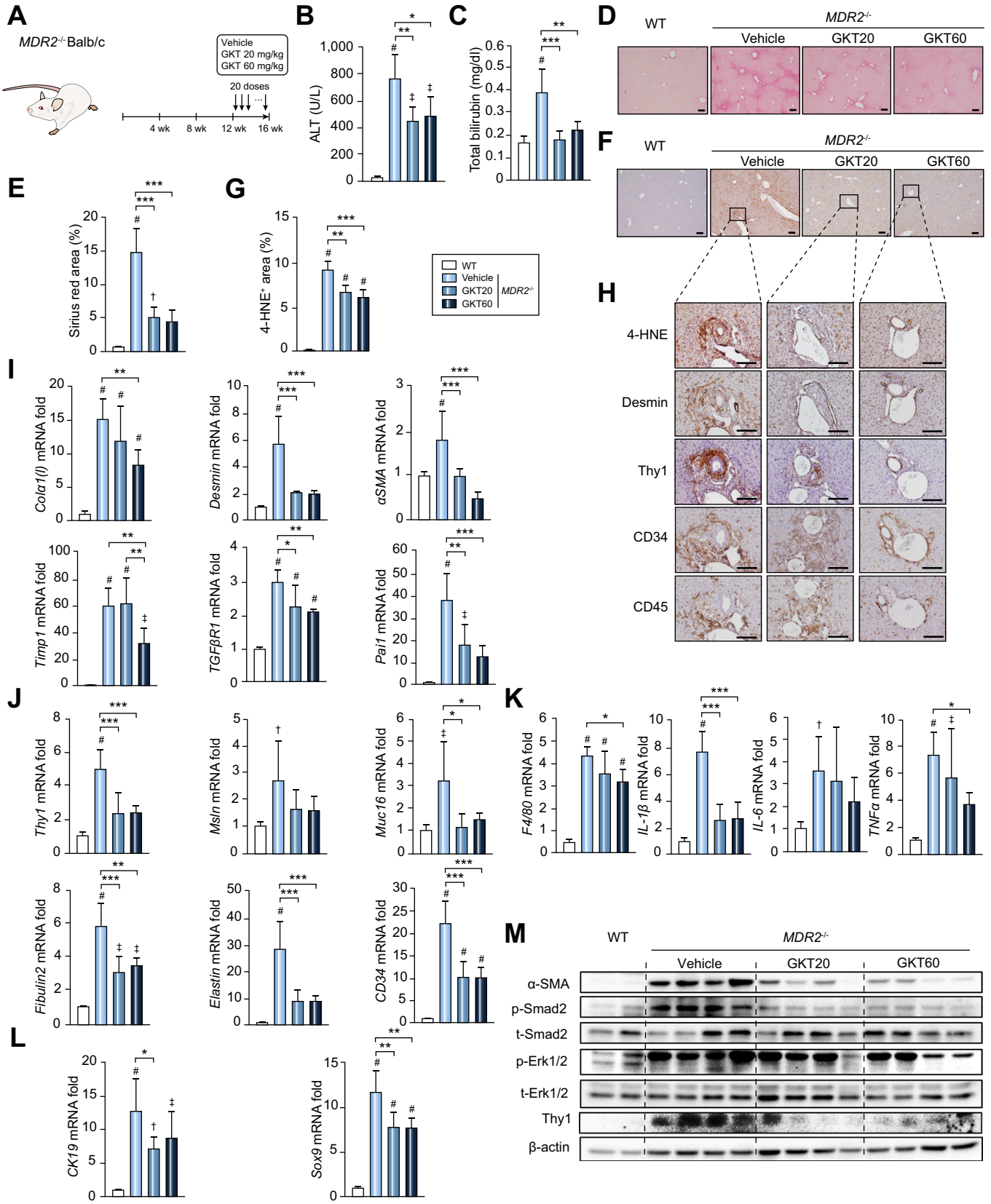

Fig. 7. Administration of NOX1/4 inhibitor attenuates cholestatic fibrosis in *Mdr2*$^{-/-}$ mice. (A) Twelve-week-old male *Mdr2*$^{-/-}$ mice were treated with 20 doses of GKT137831 (20 mg/kg [GKT20] or 60 mg/kg [GKT60]) or vehicle. Mice were sacrificed at 16 weeks old. (B) Serum levels of ALT and (C) total bilirubin. (D) Livers were stained with Sirius Red. Scale bar: 200 μm. (E) Positive area was calculated as percent. (F) Livers were stained for 4-HNE. Scale bar: 200 μm. (G) Positive area was calculated as percent. (H) Serial liver sections were stained for Desmin, Thy1, CD34, or CD45. (I) Expression of fibrogenic genes, (J) aPF markers, (K) inflammatory genes, and (L) cholangiocyte markers were analyzed by qPCR. Data are fold induction compared with 16-week-old WT mice. (M) Expression of αSMA, Smad2, Erk1/2, and Thy1 in liver was analyzed using Western blot; n = 6 per group, mean ± SD. $^{\dagger}p$ <0.05, $^{\ddagger}p$ <0.01, $^{\#}p$ <0.001 *vs.* WT; $^{*}p$ <0.05, $^{**}p$ <0.01, $^{***}p$ <0.001 by ANOVA. aPF, activated portal fibroblast; WT, wild-type.

improved liver function (≈↓1.5-fold ALT and bilirubin; Fig. 7B and C); effectively downregulated histological markers *4-HNE*, *Desmin*, *Thy1*, *CD34*, *CD45*, *PanCK*, and *Sox9* expression; and reversed pericentral fibrosis (Fig. 7D–H; Supplementary Fig. S9). This effect was accompanied by reduced (≈↓2-fold) expression of all major fibrogenic markers (*Col1a1*, *α-SMA*, *PAI1*, and *TIMP1*), aPF-specific markers (*Thy1*, *Msln*, *Muc16*, *Fibulin*, *Elastin*, and *CD34*), and cholangiocyte markers (*PanCK* and *Sox9*), as detected by qPCR (Fig. 7I–L). In a protein assay using Western blot, the administration of the NOX1/4 inhibitor significantly attenuated the αSMA and Thy1 upregulation with reduced activation of Smad2 and Erk1/2 pathway (Fig. 7M). To further address the specific effect of the NOX inhibitor on aHSCs and aPFs, we additionally performed *in vitro* studies, in which HSCs and PFs stimulated by TGFβ1 were treated with the NOX1/4 inhibitor. The administration of the NOX1/4 inhibitor significantly attenuated the expression of pro-fibrogenic markers (Supplementary Fig. S10A) as well as *NOX* genes (Supplementary Fig. S10B) in both HSCs and PFs.

Discussion

This study demonstrates that both aPFs and aHSCs contribute to the pathogenesis of cholestatic fibrosis in *Mdr2*$^{-/-}$ mice. APFs were mostly localized in the portal areas, while aHSCs were located in the portal, sinusoidal, and capsular areas. Consistent with a common etiology of cholestatic injury, Thy1^{+}Col^{GFP+} aPFs in *Mdr2*$^{-/-}$ mice exhibited a phenotype similar to that observed in aPFs in the BDL model.[14] APFs were located in close proximity to proliferating bile ducts, but cholangiocytes themselves did not express collagen type I. Although the activation of PFs was preceded by the recruitment of CD45^{+} and GR1^{+} myeloid cells to the portal areas, Col^{GFP+}CD45^{+} fibrocytes minimally contributed to ECM deposition in livers of *Mdr2*$^{-/-}$ mice. We concluded that aPFs and aHSCs are the primary targets for antifibrotic therapy. Activation of NOXs is a common mediator fibrosis in multiple organs and multiple models, and plays a critical role in the activation of aHSCs. Here, we demonstrate that NOXs are upregulated not only in aHSCs, but also in aPFs in the livers of *Mdr2*$^{-/-}$ mice. Therapeutic blocking of NOX1/4 reversed the myofibroblast activation and liver fibrosis in *Mdr2*$^{-/-}$ mice, suggesting that blocking of NOX1 and NOX4 might provide a novel target for the treatment of cholestatic fibrosis.

Cholestatic injury in *Mdr2*$^{-/-}$ mice is caused by the damage to hepatocytes (which lack functional canaliculus),[6] leading to toxic-bile-related inflammation and damage to biliary epithelium.[7] The activation of PFs is accompanied by progressive pericholangitis and cholangiocyte proliferation. Most PanCK^{+} and Sox9^{+} bile ducts were surrounded by Thy1^{+} aPFs, suggesting that aPFs may play a key role in the maintenance of the structure and integrity of the biliary tree, regulating cholangiocyte proliferation, and maintaining their polarity.[17,30,31] Although aHSCs were also detected in the portal areas, most aHSCs were located in the pericentral, sinusoidal, and capsular areas in the livers of *Mdr2*$^{-/-}$ mice. In comparison, very few aPFs were scattered throughout the sinusoidal or capsular area, suggesting that specific distribution of different cell types is associated with their distinct roles during the development of cholestatic fibrosis in *Mdr2*$^{-/-}$ mice.[16] In support, we identified a unique population of CD45^{+} and Gr1^{+} cells populating periductular areas at the very onset of cholestatic injury in *Mdr2*$^{-/-}$ mice. Some of these Gr1^{+} cells directly infiltrated into the bile duct structures, and were located underneath or between cholangiocytes, suggesting that they might play a critical role in the regulation of ductular proliferation and/or activation of PFs. Mdr2 deficiency has been reported to induce the disruption of the basement membrane of cholangial duct, leading to the leakage of bile acid into the periductal space.[7] We can speculate that the CD45^{+} and Gr1^{+} neutrophils migrated in response to early injury of cholangiocytes and bile acid leakage, causing acute inflammation and subsequent expansion of periportal myofibroblasts.

Our current study evaluated the dynamic age-dependent changes in histological and mRNA expression of cell-specific markers during the development of cholestatic fibrosis in *Mdr2*$^{-/-}$ mice. To support our histological findings, widely used reporter collagen-1α(1)-GFP mice were used to visualize collagen type I-expressing myofibroblasts. In contrast to previous reports,[27] here, we demonstrate that PanCK^{+} or Sox9^{+} cholangiocytes did not upregulate Collagen Type I in livers of *Mdr2*$^{-/-}$ mice. Furthermore, *Desmin* has been previously considered as an HSC-specific marker. Based on our analysis, *Desmin* positive staining was co-localized in approximately 36% of Thy1^{+} aPFs and Thy1^{-} aHSCs. As this result could be attributed to a non-specific immunoreactivity of anti-Desmin Ab, we examined the livers from reporter Lrat^{YFP} mice, which are used for lineage tracing of HSCs. We demonstrated that, in mice expressing constitutive Lrat^{YFP}, 46% of Thy1^{+} aPFs were marked with Lrat^{YFP}, and 73% of Desmin^{+} cells were marked with Lrat^{YFP}, suggesting that Lrat^{Cre} does not discriminate between aPFs and HSCs. This fact would explain why Mederacke *et al.*[15] did not identify aPFs as a population distinct from aHSCs that contributes to cholestatic fibrosis in Lrat^{YFP} mice. In adult mice, *Lrat* is expressed in HSCs and not PFs.[2,15] Given the mesenchymal origin of both aPFs and aHSCs, the expression of *Lrat* during embryonic development might result in genetic labeling of both PF and HSC populations in Lrat^{YFP} mice. *Lrat* is also expressed in extrahepatic tissues, including the lung and retina.[32] Such common markers as *Desmin* and *Lrat* may be expressed in myofibroblasts originating from either HSCs or PFs, suggesting that new markers are needed to discriminate between aPFs and aHSCs. Thus, the contribution of aPFs in *Mdr2*$^{-/-}$ mice might have been masked by using the conventional markers for HSCs, including Desmin and Lrat^{YFP}. In this study, the marker Thy1, expression of Type I collagen, absence of vitamin A, and the characteristic localization have revealed the significant role of aPFs in cholestatic fibrosis.

Furthermore, we identified that a subset of Thy1^{+}Col^{GFP+} aPFs co-expressed CD34. CD34^{+} cells located in a portal area exhibited a myofibroblast-like shape. Expansion of CD34^{+}Col^{GFP+} aPFs was a unique feature of cholestatic liver fibrosis, as demonstrated by the upregulation of CD34^{+}Col^{GFP+} aPFs in *Mdr2*$^{-/-}$ and BDL-injured mice, and was not observed in livers of CCl_4-injured mice. Our data suggest that CD34 is another marker of aPFs in adult mice. In support, expression of CD34 as a marker of hepatic mesenchymal progenitor cells was previously suggested.[28] Follow-up studies are needed to determine the functional properties of Thy1^{+}CD34^{+} and Thy1^{+}CD34^{-} aPFs.

Bone-marrow-derived fibrocytes are another population that can potentially give rise to myofibroblasts.[3,33] It has been reported that CD34^{+} fibrocytes of BM origin are involved in fibrosis in *Mdr2*$^{-/-}$ mice.[29] In the present study, only few CD34^{+} fibrocytes contributed to a population of Col^{GFP+} myofibroblasts.

The therapeutic properties of NOX1/4 inhibitor on liver fibrosis induced by CCl_4, BDL, and NASH models have been previously reported.[23,34] This study demonstrated the effectiveness of NOX1/4 inhibition on cholestatic fibrosis in *Mdr2*$^{-/-}$ mice. Notably, the administration of the NOX1/4 inhibitor reduced oxidative stress, activation/proliferation of aHSCs and Thy1^{+}-desmin^{+}CD34^{+} aPFs, portal infiltration with CD45^{+} cells, and cholangiocyte proliferation. Thus, we propose that the interactions between cholangiocyte injury, neutrophil migration, and PF activation are targets of NOX inhibition.

Financial support

This study was supported by the National Institutes of Health R01 DK101737-01A1, U01 AA022614-01A1, R01 DK099205-01A1, P50AA011999, and AI043477 (TK and DAB), and the Herman Lopata Memorial Hepatitis Postdoctoral ALF Fellowship (JX).

Conflict of interest

The authors declare no conflict of interest.

Please refer to the accompanying ICMJE disclosure forms for further details.

Authors' contributions

TN performed the experiments, collected and analyzed the data, and wrote the manuscript. RH, SL, YK, GY, DK, JB, H-YM, JX, XL, and DD performed the experiments. SBR analyzed the data. KI and KT provided support with data collection. TK and DAB provided support, designed the study, and wrote the manuscript.

Acknowledgements

The authors thank Philippe Wiesel and Cedric Szyndralewiez (Genkyotex S.A.) for providing GKT137831, Dennis R. Petersen for providing the antibody against 4-HNE, Ryan McCubbin and Katrin Hochrath (University of California San Diego, La Jolla, CA, USA) for their help with in vivo experiments, and Karin Diggle (University of California San Diego) for her excellent management of the laboratory.

Supplementary data

Supplementary data to this article can be found online at https://doi.org/10.1016/j.jhep.2019.04.012.

References

Author names in bold designate shared co-first authorship

[1] Bataller R, Brenner DA. Liver fibrosis. J Clin Invest 2005;115:209–218.
[2] **Iwaisako K**, **Jiang C**, **Zhang M**, Cong M, Moore-Morris TJ, Park TJ, et al. Origin of myofibroblasts in the fibrotic liver in mice. Proc Natl Acad Sci U S A 2014;111:E3297–E3305.
[3] Kisseleva T, Uchinami H, Feirt N, Quintana-Bustamante O, Segovia JC, Schwabe RF, et al. Bone marrow-derived fibrocytes participate in pathogenesis of liver fibrosis. J Hepatol 2006;45:429–438.
[4] Wells RG, Schwabe RF. Origin and function of myofibroblasts in the liver. Semin Liver Dis 2015;35:97–106.
[5] Kisseleva T, Cong M, Paik Y, Scholten D, Jiang C, Benner C, et al. Myofibroblasts revert to an inactive phenotype during regression of liver fibrosis. Proc Natl Acad Sci U S A 2012;109:9448–9453.
[6] Mariotti V, Strazzabosco M, Fabris L, Calvisi DF. Animal models of biliary injury and altered bile acid metabolism. Biochim Biophys Acta 2018;1864:1254–1261.
[7] Fickert P, Fuchsbichler A, Wagner M, Zollner G, Kaser A, Tilg H, et al. Regurgitation of bile acids from leaky bile ducts causes sclerosing cholangitis in Mdr2 (Abcb4) knockout mice. Gastroenterology 2004;127:261–274.
[8] Miethke AG, Zhang W, Simmons J, Taylor AE, Shi T, Shanmukhappa SK, et al. Pharmacological inhibition of apical sodium-dependent bile acid transporter changes bile composition and blocks progression of sclerosing cholangitis in multidrug resistance 2 knockout mice. Hepatology 2016;63:512–523.
[9] **Baghdasaryan A**, **Fuchs CD**, Österreicher CH, Lemberger UJ, Halilbasic E, Påhlman I, et al. Inhibition of intestinal bile acid absorption improves cholestatic liver and bile duct injury in a mouse model of sclerosing cholangitis. J Hepatol 2016;64:674–681.
[10] Lazaridis KN, Strazzabosco M, Larusso NF. The cholangiopathies: disorders of biliary epithelia. Gastroenterology 2004;127:1565–1577.
[11] **Fickert P**, **Pollheimer MJ**, Beuers U, Lackner C, Hirschfield G, Housset C, et al. Characterization of animal models for primary sclerosing cholangitis (PSC). J Hepatol 2014;60:1290–1303.
[12] **Wan Y**, **Meng F**, Wu N, Zhou T, Venter J, Francis H, et al. Substance P increases liver fibrosis by differential changes in senescence of cholangiocytes and hepatic stellate cells. Hepatology 2017;66:528–541.
[13] Meng F, Kennedy L, Hargrove L, Demieville J, Jones H, Madeka T, et al. Ursodeoxycholate inhibits mast cell activation and reverses biliary injury and fibrosis in Mdr2. Lab Invest 2018;98:1465–1477.
[14] Koyama Y, Wang P, Liang S, Iwaisako K, Liu X, Xu J, et al. Mesothelin/mucin 16 signaling in activated portal fibroblasts regulates cholestatic liver fibrosis. J Clin Invest 2017;127:1254–1270.
[15] Mederacke I, Hsu CC, Troeger JS, Huebener P, Mu X, Dapito DH, et al. Fate tracing reveals hepatic stellate cells as dominant contributors to liver fibrosis independent of its aetiology. Nat Commun 2013;4:2823.
[16] Wells RG. The portal fibroblast: not just a poor man's stellate cell. Gastroenterology 2014;147:41–47.
[17] Jhandier MN, Kruglov EA, Lavoie EG, Sévigny J, Dranoff JA. Portal fibroblasts regulate the proliferation of bile duct epithelia via expression of NTPDase2. J Biol Chem 2005;280:22986–22992.
[18] European Association for the Study of the Liver. EASL clinical practice guidelines: management of cholestatic liver diseases. J Hepatol 2009;51:237–267.
[19] Paik YH, Iwaisako K, Seki E, Inokuchi S, Schnabl B, Osterreicher CH, et al. The nicotinamide adenine dinucleotide phosphate oxidase (NOX) homologues NOX1 and NOX2/gp91(phox) mediate hepatic fibrosis in mice. Hepatology 2011;53:1730–1741.
[20] Cui W, Matsuno K, Iwata K, Ibi M, Matsumoto M, Zhang J, et al. NOX1/nicotinamide adenine dinucleotide phosphate, reduced form (NADPH) oxidase promotes proliferation of stellate cells and aggravates liver fibrosis induced by bile duct ligation. Hepatology 2011;54:949–958.
[21] Bataller R, Schwabe RF, Choi YH, Yang L, Paik YH, Lindquist J, et al. NADPH oxidase signal transduces angiotensin II in hepatic stellate cells and is critical in hepatic fibrosis. J Clin Invest 2003;112:1383–1394.
[22] De Minicis S, Seki E, Oesterreicher C, Schnabl B, Schwabe RF, Brenner DA. Reduced nicotinamide adenine dinucleotide phosphate oxidase mediates fibrotic and inflammatory effects of leptin on hepatic stellate cells. Hepatology 2008;48:2016–2026.
[23] Aoyama T, Paik YH, Watanabe S, Laleu B, Gaggini F, Fioraso-Cartier L, et al. Nicotinamide adenine dinucleotide phosphate oxidase in experimental liver fibrosis: GKT137831 as a novel potential therapeutic agent. Hepatology 2012;56:2316–2327.
[24] **Hochrath K**, **Krawczyk M**, Goebel R, Langhirt M, Rathkolb B, Micklich K, et al. The hepatic phosphatidylcholine transporter ABCB4 as modulator of glucose homeostasis. FASEB J 2012;26:5081–5091.
[25] Yata Y, Scanga A, Gillan A, Yang L, Reif S, Breindl M, et al. DNase I-hypersensitive sites enhance alpha1(I) collagen gene expression in hepatic stellate cells. Hepatology 2003;37:267–276.
[26] Seki E, De Minicis S, Osterreicher CH, Kluwe J, Osawa Y, Brenner DA, et al. TLR4 enhances TGF-beta signaling and hepatic fibrosis. Nat Med 2007;13:1324–1332.
[27] Lua I, Li Y, Zagory JA, Wang KS, French SW, Sévigny J, et al. Characterization of hepatic stellate cells, portal fibroblasts, and mesothelial cells in normal and fibrotic livers. J Hepatol 2016;64:1137–1146.
[28] Chauhan H, Abraham A, Phillips JR, Pringle JH, Walker RA, Jones JL. There is more than one kind of myofibroblast: analysis of CD34 expression in benign, in situ, and invasive breast lesions. J Clin Pathol 2003;56:271–276.

[29] **Roderfeld M**, **Rath T**, Voswinckel R, Dierkes C, Dietrich H, Zahner D, et al. Bone marrow transplantation demonstrates medullar origin of CD34+ fibrocytes and ameliorates hepatic fibrosis in Abcb4 mice. Hepatology 2010;51:267–276.
[30] Lorena D, Darby IA, Reinhardt DP, Sapin V, Rosenbaum J, Desmoulière A. Fibrillin-1 expression in normal and fibrotic rat liver and in cultured hepatic fibroblastic cells: modulation by mechanical stress and role in cell adhesion. Lab Invest 2004;84:203–212.
[31] Li Z, Dranoff JA, Chan EP, Uemura M, Sévigny J, Wells RG. Transforming growth factor-beta and substrate stiffness regulate portal fibroblast activation in culture. Hepatology 2007;46:1246–1256.
[32] Liu L, Gudas LJ. Disruption of the lecithin:retinol acyltransferase gene makes mice more susceptible to vitamin A deficiency. J Biol Chem 2005;280:40226–40234.
[33] **Forbes SJ**, **Russo FP**, Rey V, Burra P, Rugge M, Wright NA, et al. A significant proportion of myofibroblasts are of bone marrow origin in human liver fibrosis. Gastroenterology 2004;126:955–963.
[34] **Bettaieb A**, **Jiang JX**, Sasaki Y, Chao TI, Kiss Z, Chen X, et al. Hepatocyte nicotinamide adenine dinucleotide phosphate reduced oxidase 4 regulates stress signaling, fibrosis, and insulin sensitivity during development of steatohepatitis in mice. Gastroenterology 2015;149(468–80) e410.